STATIC AEROELASTIC ANALYSIS OF COMPOSITE WING

ICAS-90-1.4.2

In Lee*, Seung Ho Kim** and Chang Sun Hong***
Dept. of Aerospace Eng
Korea Advanced Institute of Science and Technology
Seoul, Korea

Hirokazu Miura#
NASA Ames Research Center, Moffet Field, CA 94035, U.S.A

Abstract

A static aeroelastic analysis capability that can predict aerodynamic loads for the deformed shape of the composite wing has been developed. The finite element method(FEM) was used for composite plate structural analysis, and the linear vortex lattice method(VLM) was used for steady aerodynamic analysis. The final deformed shape of the wing due to applied forces is determined by iterative manner using FEM and VLM. FEM and VLM analysis are related by a surface spline interpolation procedure. The wing with Gr/Ep composite material has been investigated to see the wing deformation effect. Aerodynamic load change due to wing flexibility has been investigated. Also, the effect of fiber orientation and sweep angle on the deformation pattern and aerodynamic coefficients are examined. For a certain fiber orientation, the deflection and aerodynamic loading of the composite wing is very much reduced. The swept forward wing has more significant effect of wing flexibility on aerodynamic coefficient than the swept back wing does.

Introduction

A static aeroelasticity is a problem involving the response of a flexible structure to aerodynamic loading. The static aeroelasticity is increasingly being considered as a primary design parameter , affecting as it does structural optimization, vehicle aerodynamic stability, control effectiveness, and overall performance[1]. The analysis of static aeroelasticity involves calculation of a static response including loads and stresses in the structure.

Recent development in laminated composite materials enables us to make more lighter aircraft structures which have enough strength without further increase in weight[2]. Many aeroelastic researches have been performed for flutter and divergence analysis of a composite wing related with aeroelastic tailoring. The most important thing in the design of an aircraft wing structure involving aeroelastic tailoring is to get accurate aerodynamic load distribution considering elastic deformation.

In most aeroelastic studies, the computation of aerodynamic loads to consider elastic deformation of a wing depends mainly on simple theories. A wing structure have been modelled by a cantilevered beam or a box beam. Many previous investigators have used aerodynamic strip theory as aerodynamic tools[3-7]. This theory gives good results for a large aspect ratio wing. However, for a more complex realistic wings, the theory is not appropriate. To get more accurate aeroelastic load for more complex wing structure, numerical tools like the finite element method and many computational fluid dynamics techniques are introduced. Doublet lattice method and other panel method based on linearized potential theories have been used to get accurate aeroelastic loads in subsonic and supersonic flow region[1,8-10]. For transonic flow regime, more advanced computational fluid dynamic technic is used to obtain aerodynamic load distributions[11-13]. For structural analysis, the finite element method is used for analyzing more complex structures. Many studies have been performed for aeroelastic analysis of the composite wing about flutter and divergence calculations[2,4-10]. However, they do not give proper information of the interaction between a wing structure and aerodynamic flow fields. In the initial design phase of the composite wing, it is required to know the deformation pattern and aerodynamic load change due to the flexibility of the composite wing.

The main objective of this study is to get the aerodynamic load change due to the flexibility of the composite wing. Also, the effect of the fiber orientation on the deformation pattern and aerodynamic coefficients are examined. In this paper, a wing structure is assumed as a plate-like wing. The finite element method for a laminated composite plate which accounts for the transverse shear deformation is used for the structural analysis. For the aerodynamic load calculation, the vortex lattice method[14] is applied to the various shaped thin wings. The finite element method and the vortex lattice method are combined by the surface spline method[15]. The deformed shape of a wing and re-distributed aerodynamic forces are obtained from the iteration

---

* Assistant Professor
** Graduate Student
*** Professor
\# Research Scientist

procedure of the finite element method and the vortex lattice method. Various shaped thin wings are analyzed in this analysis. Parametric studies on the sweep angle, the fiber orientation and the free stream velocity are performed to see the flexibility effect of the laminated composite wing.

Analysis

In the calculation of aerodynamic load, it is assumed that the wing is a lifting surface with thin airfoil, and the flow is incompressible and in the low subsonic range. Structurally, the wing is assumed as a thin plate. The deformed wing configuration is determined through the iteration procedure. Initially, the aerodynamic forces on the undeformed wing are calculated by the linear vortex lattice panel method. These aerodynamic forces are interpolated to the finite element nodal forces. Thus, the deformed wing configuration is determined by the finite element equation. The aerodynamic forces on the deformed wing are again calculated. Iteration procedure is performed until the final equilibrium state is reached.

Finite Element Method

In this study, the finite element method is applied for the structural analysis of the anisotropic composite plate. The classical laminated plate theory that does not includes transverse shear deformation requires the C^1-continuity of the finite element. In this finite element formulation, the transverse shear deformation is included. Thus, C^0-continuity element can be used.

Integration of the equilibrium equation neglecting body forces gives the governing equations for the symmetrically laminated composite plate[16].

$$\frac{\partial}{\partial x}\left[A_{45}\left(\frac{\partial w}{\partial y}+\phi_y\right)+A_{55}\left(\frac{\partial w}{\partial x}+\phi_x\right)\right]+\frac{\partial}{\partial y}\left[A_{44}\left(\frac{\partial w}{\partial y}+\phi_y\right) + A_{45}\left(\frac{\partial w}{\partial x}+\phi_x\right)\right]+q=0 \tag{1}$$

$$\frac{\partial}{\partial x}\left[D_{11}\frac{\partial \phi_x}{\partial x}+D_{12}\frac{\partial \phi_y}{\partial y}+D_{16}\left(\frac{\partial \phi_x}{\partial y}+\frac{\partial \phi_y}{\partial x}\right)\right]+\frac{\partial}{\partial y}\left[D_{16}\frac{\partial \phi_x}{\partial x}+D_{26}\frac{\partial \phi_y}{\partial y} + D_{66}\left(\frac{\partial \phi_x}{\partial y}+\frac{\partial \phi_y}{\partial x}\right)\right]-A_{45}\left(\frac{\partial w}{\partial y}+\phi_y\right)-A_{55}\left(\frac{\partial w}{\partial x}+\phi_x\right)=0 \tag{2}$$

$$\frac{\partial}{\partial x}\left[D_{16}\frac{\partial \phi_x}{\partial x}+D_{26}\frac{\partial \phi_y}{\partial y}+D_{66}\left(\frac{\partial \phi_x}{\partial y}+\frac{\partial \phi_y}{\partial x}\right)\right]+\frac{\partial}{\partial y}\left[D_{12}\frac{\partial \phi_x}{\partial x}+D_{22}\frac{\partial \phi_y}{\partial y} + D_{26}\left(\frac{\partial \phi_x}{\partial y}+\frac{\partial \phi_y}{\partial x}\right)\right]-A_{44}\left(\frac{\partial w}{\partial y}+\phi_y\right)-A_{45}\left(\frac{\partial w}{\partial x}+\phi_x\right)=0 \tag{3}$$

In this study, the variables for FEM analysis are the transverse displacement w, and two rotation angles ϕ_x and ϕ_y with respect to y and x axis, respectively. The coordinate system is given in Fig. 1. Multiplying weight function $\bar{\psi}_i$ (i=1, 2, 3) to (1)~(3), and integrating them in the arbitrary region Ω_e, we can obtain the weak form of the finite element. The variables ϕ_x, ϕ_y and w are approximated by the shape functions.

$$w=\sum_{i=1}^{n} w_i\psi_i,\quad \phi_x=\sum_{i=1}^{n}\phi_x^i\psi_i,\quad \phi_y=\sum_{i=1}^{n}\phi_y^i\psi_i \tag{4}$$

Let $\bar{\psi}_\alpha=\psi_i$ (α=1, 2, 3). Then, we get the following finite element equation from eq. (1)~(3).

$$\begin{bmatrix} [K^{11}] & [K^{12}] & [K^{13}] \\ & [K^{22}] & [K^{23}] \\ \text{sym.} & & [K^{33}] \end{bmatrix}\begin{Bmatrix}\{w\}\\ \{\phi_x\}\\ \{\phi_y\}\end{Bmatrix}=\begin{Bmatrix}\{F^1\}\\ \{F^2\}\\ \{F^3\}\end{Bmatrix} \tag{5}$$

The elements of the stiffness matrix [K] are listed in appendix. Here, the force vectors are obtained from the surface spline transformation of the aerodynamic forces which are calculated from the VLM method. The elements of the stiffness matrix can be calculated by Gaussian quadrature. In terms containing transverse shear deformation i.e., the terms containing A_{45}, A_{44}, and A_{55}, there occurs so called locking phenomena for a thin plate. So, the displacements are not calculated correctly. Therefore reduced integration must be used to solve this problem[17]. In this paper, the four node isoparametric element was used to calculate the stiffness matrix. The Gaussian integration of 2×2 points was used, and 1×1 point for reduced integration.

Vortex Lattice Method

The wing surface is divided into many lattices in the vortex lattice method. Each lattice is considered as a small lifting surface. The interaction between each lattice is represented by a linear equations. Each lattice consists of the bound vortex, free vortex, and the control point where the boundary condition is applied. From the Biot-Savart law, the velocity $V_{m,n}$ induced by the vortex element which has the strength Γ_n is represented as follows[14].

$$\vec{V}_{m,n}=\vec{C}_{m,n}\,\Gamma_n \tag{6}$$

The total velocity at m-th control point is obtained by adding the free stream velocity and the velocity induced from 2N vortex system.

$$\vec{V}_m=\vec{U}_\infty+\sum_{n=1}^{2N} V_{m,n} \tag{7}$$

The vortex strength Γ_n can be determined from the condition that there are no velocity components normal to the wing surface at the control points.

$$\sum_{n=1}^{2N} [\vec{C}_{m,n} \cdot \vec{n}_m] \{\Gamma_n\} = -\{\vec{U}_\infty \cdot \vec{n}_m\} \quad (8)$$

When Γ_n is known, Kutta-Joukowski theorem gives the lift acting on the vortex of each lattice.

$$l_n = \rho_\infty U_\infty \Gamma_n \Delta y_n \quad (9)$$

where, l_n is the lift force acting on each lattice, ρ_∞ is the density of the free stream air and, Δy_n is the length of a bound vortex in each lattice.

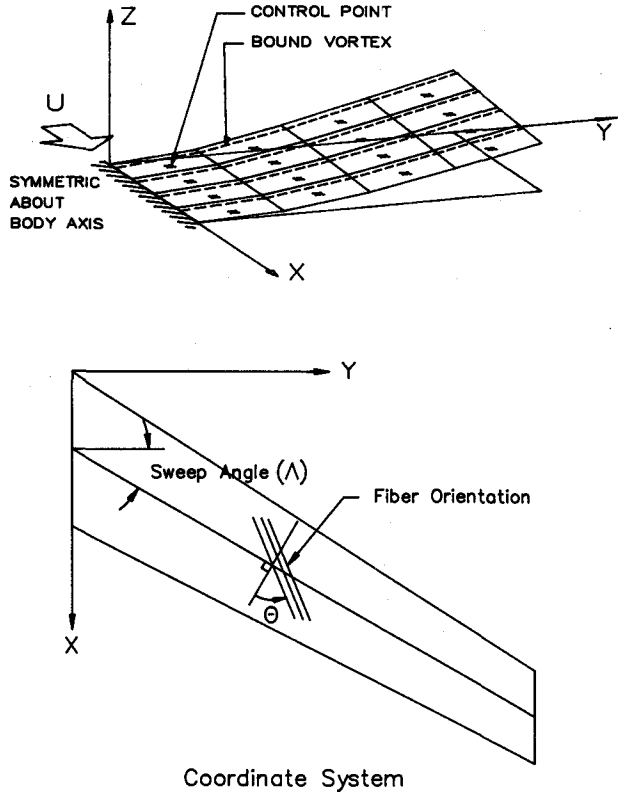

Fig.1 Coordinate System and Wing Modeling.

Surface Spline Method

The grid system of the finite element method and the vortex lattice method do not necessarily coincide. The surface spline method[15] has been used to match the forces and the displacements of the two different grid systems. Basic concept of the surface spline is to get the surface of an infinite plate deformed by a point force.

The relation between FEM structural displacement $\{u_g\}$ and VLM lattice displacement $\{u_k\}$ can be obtained.

$$\{u_k\} = [G_{kg}]\{u_g\} \quad (10)$$

where $[G_{kg}]$ is the interpolation matrix between two displacements.

The lift forces acting on the center of the bound vortex must be converted to the finite element nodal forces. The virtual work done by aerodynamic forces is equal to the virtual work done by the nodal forces of the finite element . Therefore, we can derive the following relation.

$$\{u_k\}^T \{F_k\} = \{u_g\}^T \{F_g\} \quad (11)$$

From (10), we get the following relations.

$$\{u_k\}^T = \{u_g\}^T [G_{kg}]^T.$$

$$\{F_g\} = [G_{kg}]^T \{F_k\} \quad (12)$$

Hence, aerodynamic forces are converted to finite element nodal forces by the above relation.

Results and Discussion

Three types of wings (sweep angle 0°,30°,-30°) have been investigated to see the wing flexibility effect. The wing modeling and the coordinate system are shown in Fig. 1. Numerical computation was performed for a right side wing due to wing symmetry. The boundary condition used in FEM analysis is the clamped condition at the wing root. However, the total wing was considered in VLM analysis since there is interaction between the left and the right wing. T300/5208 Gr/Ep Composite material was used for the computation, and the material property and wing dimension are given as belows.

$E_1 = 20.0 \times 10^6$ psi, $E_2 = 1.40 \times 10^6$ psi

$G_{12} = G_{13} = 0.8 \times 10^6$ psi, $G_{23} = 0.6 \times 10^6$ psi, $\nu_{12} = 0.3$

Half Wing Span = 15 in., Chord = 5 in.

Taper ratio = 0.6, Ply Thickness = 4.92×10^{-3} in.

The grid system for a 30° swept back wing is shown in Fig. 2. The grid systems of the other wings were modelled in a similar manner. The number of aerodynamic panels is 200 (10 × 20) for the right side wing alone. Since there is the stiff gradient of pressure near wing leading edge and wing tip, fine meshes were used there as shown in Fig. 2. The number of finite elements used were 120 (8 × 15) for the right side wing.

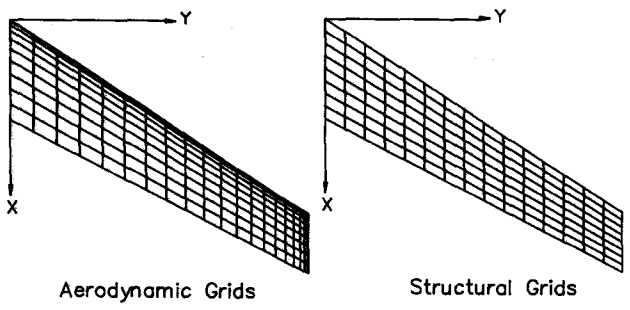

Fig.2 Grid Systems of 30° Swept Back Wing.

The iteration numbers of computation in this study are about 5~30. When the stiffnesses of the wing is small, the computation requires many iterations. For the wash-in type deformation, the deflection increases monotonically to the converged value. For the wash-out type deformation, the convergence history is oscillatory.

Verification of Computer Code

For verifying the computer code used, comparison was made with the results of Landsberger and Dugundji[7]. A straight rectangular wing with a stacking sequence $[120_2/90]_S$ was used to examine the wing deflection at various angle of attack and air speed. The result is shown in Fig. 3. The present computer code gives relatively accurate results in the low velocities (5 and 11.5 m/s). In the higher air speed(16m/s), the present code predicts smaller value than the result of Landsberger and Dugundji, but gives acceptable results. From this results, we can say that the present computer code gives reasonable results. In the present analysis, the free stream air velocity is chosen so that the wing deflection is not larger than 10 percent of the wing span length.

The Effects of Fiber Orientation on Deformation Pattern

A T300/5208 Graphite/Epoxy composite wing with a stacking sequence of $[\theta_2/90_2]_S$ has been analyzed. The computation was performed for various fiber orientation. The bending stiffness coefficients are shown in Fig.4. D_{11} and D_{22} are the bending stiffnesses about y and x axis, respectively. D_{66} represents the torsional stiffness , and D_{12} is the coupling stiffness for bending to bending. D_{16} and D_{26} represents the coupling stiffnesses for bending and torsion.

The deformed patterns for three types of wing are shown at Fig.5~7. For the unswept wing, the wash-out deformation is observed in θ = 105°~150°. In these fiber orientations, the

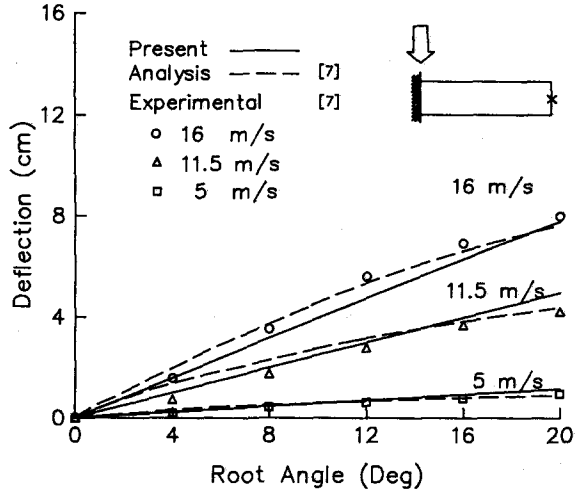

Fig.3 Comparison of the Steady Airload Deflection of $[120_2/90]_S$ Rectangular Wing with the Result of Landsberger[7].

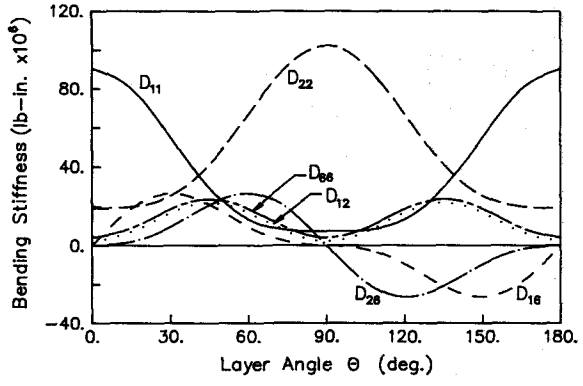

Fig.4 Bending Stiffnesses of $[\theta_2/90_2]_S$ Laminate.

effect of coupling stiffnesses is dominant as shown in Fig. 4. For the other fiber orientation, the wash-in deformation is observed. The deformation pattern for a 30° swept back wing is shown in Fig. 6. In the swept back wing, the wash-out is the general deformation pattern. However, the wash-in is observed at θ = 60°~90° due to the coupling stiffness term. The deformation pattern of a 30° swept forward wing is shown in Fig. 7. In the swept forward wing, the wash-in occurs dominantly because the wing loading near the leading edge makes larger twisting moment . When proper fiber orientation (θ = 105°~120°) is used, the wash-in deformation can be very much reduced. When θ =105° a small wash-out deformation is observed. When θ = 75°, the greatest torsional deformations are observed for three cases, because of the small bending stiffnesses and the large coupling stiffnesses.

Fig. 8~10 show the wing tip deflection for the above cases.

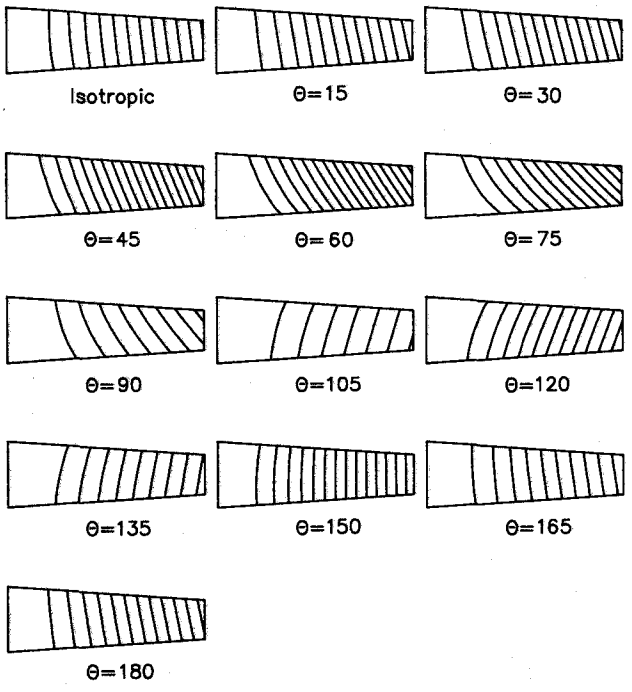

Fig.5 Contour Plot of Deformed Shape for $[\theta_2/90_2]_S$ Unswept wing ($\Lambda = 0°$, $U_\infty = 600$ in./s, $\alpha = 2°$).

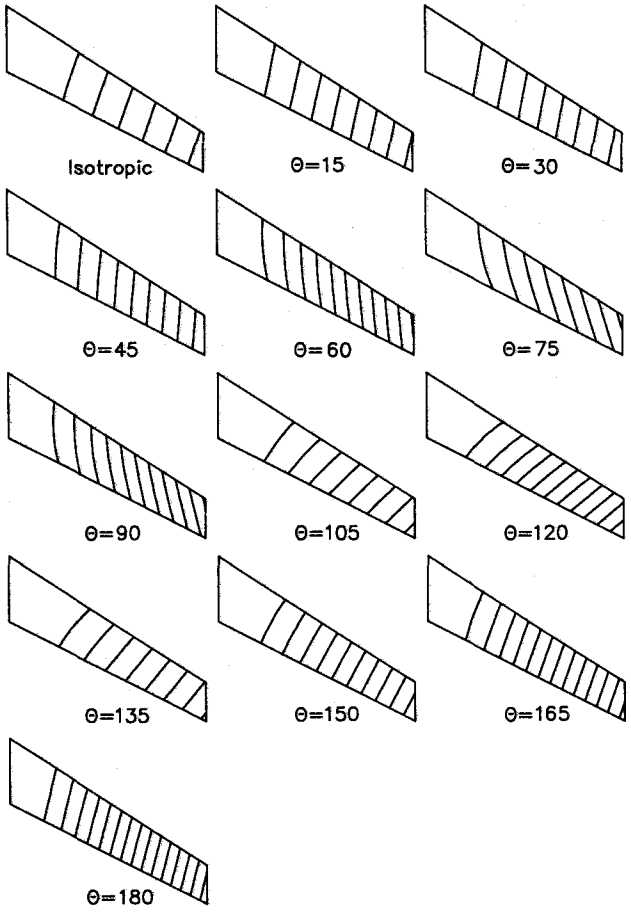

Fig.6 Contour Plot of Deformed Shape for $[\theta_2/90_2]_S$ Swept Back Wing ($\Lambda = 30°$, $U_\infty = 600$ in./s, $\alpha = 2°$).

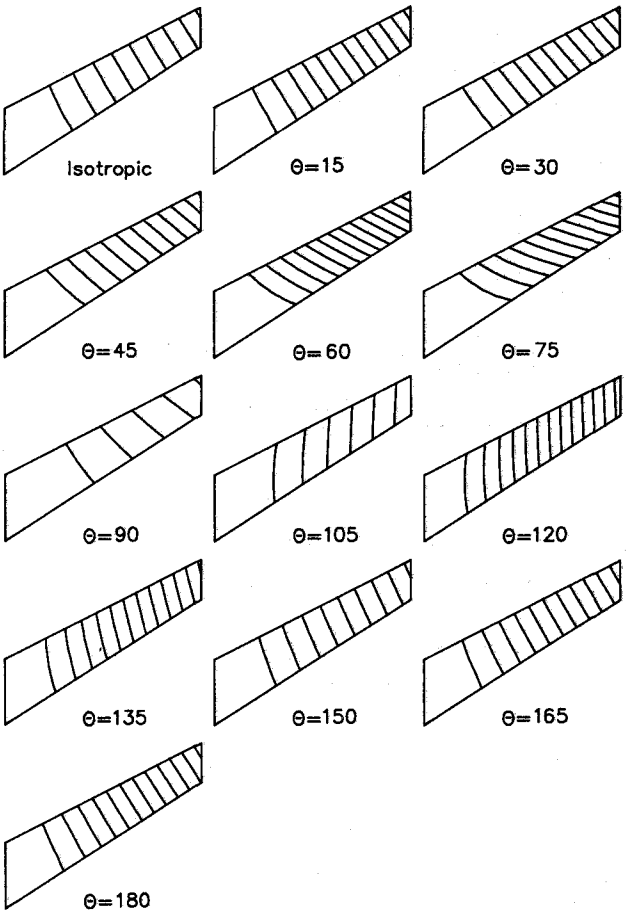

Fig.7 Contour Plot of Deformed Shape for $[\theta_2/90_2]_S$ Swept Forward Wing.($\Lambda = -30°$, $U_\infty = 400$ in./s, $\alpha = 2°$).

For the unswept wing, maximum deflection occurs near θ = 45°. In this fiber orientation, the bending stiffnesses are small and the effect of coupling stiffnesses enforces the wash-in phenomena. When θ = 90°~120°, smaller deflection can be observed due to both the large bending stiffnesses D_{22} and the effect of coupling stiffnesses. The tip deflection pattern of the swept back wing and the swept forward wing (Fig.9,10) can be explained in the same manner as in the unswept wing. However, the geometry effect and the different aerodynamic loading give different deformation patterns. It is noticeable for the above three cases that the deflection can be reduced in a favorable manner when θ = 80°~120°. For the prevention of divergence, it is recommended that the wing deformation must be in these regions. For the swept forward wing, the wash-out phenomena hardly occur, but the torsional deformation can be properly reduced by selecting the proper fiber orientation (θ = 90°~120°).

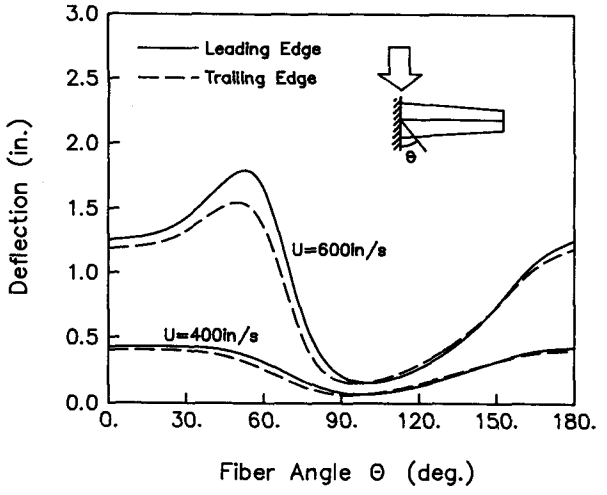

Fig.8 Effect of Fiber Orientation θ upon Tip Deflections of $[\theta_2/90_2]_S$ Unswept Wing ($\Lambda = 0°$, $\alpha = 2°$).

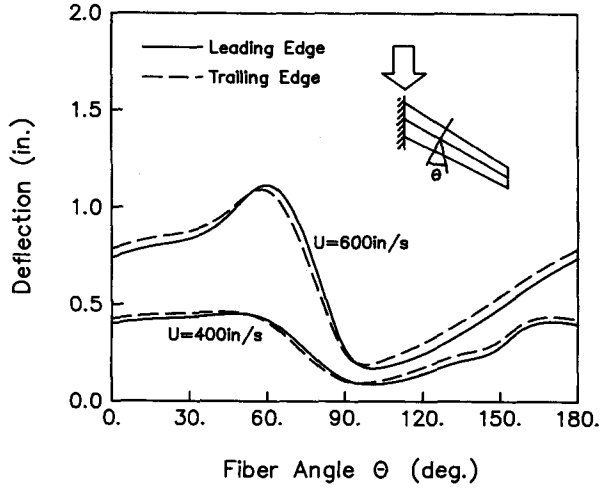

Fig.9 Effect of Fiber Orientation θ upon Tip Deflections of $[\theta_2/90_2]_S$ Swept Back Wing ($\Lambda = 30°, \alpha = 2°$).

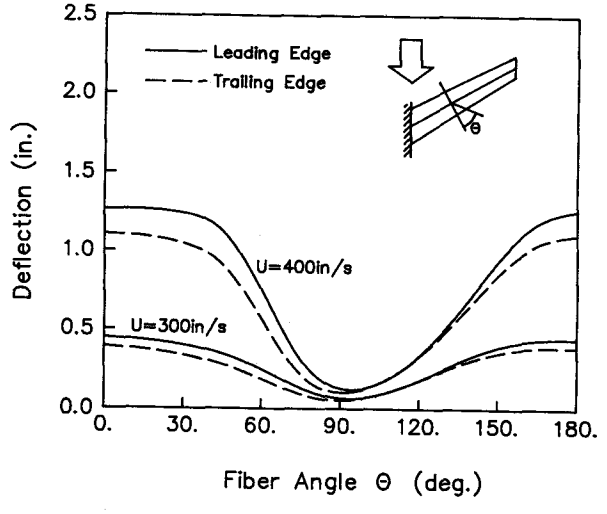

Fig.10 Effect of Fiber Orientation θ upon Tip Deflections of $[\theta_2/90_2]_S$ Swept Forward Wing ($\Lambda = -30°, \alpha = 2°$).

The Effects of Fiber Orientation on Aerodynamic forces

The wing deformation due to the fiber orientation is coupled with aerodynamic forces acting on the wing. The elastic effects on the total lift coefficients are examined for three wings. The results are shown in Fig. 11~13. For the unswept wing (Fig. 11), large lift is developed at $\theta = 60°$ due to large wing deformation. When $\theta = 100°$~$140°$, lift coefficients are smaller than those of the rigid wing because of the wash-out effect. For the other fiber angles, larger lift forces are developed due to the wash-in deformation. At $\theta = 105°$ and $150°$, the lift coefficients approach those of the rigid wing. Although the deflection at $\theta = 150°$ is much larger than that of $\theta = 105°$, the lift coefficient is almost the same because of the similar torsional deformation patterns. We can see the significance of local angle of attack change as a result of torsional deformation. For the 30° swept back wing, the lift coefficient at $\theta = 45°$~$90°$ are larger than those of the rigid wing due to the wash-in deformation. In the other fiber angles, smaller lift is observed due to the wash-out deformation and lift coefficients are smaller than those of the rigid wing. The effect of velocity change is not so large compared with the other wing cases. For the swept forward wing, we can see that the lift coefficient approaches to that of the rigid wing case at $\theta = 90°$~$120°$. In the forward swept wing, small increase in velocity produces large increase in lift. For any fiber orientation, the lift is always larger than that of the rigid wing.

the spanwise lift variation for various fiber orientation is given in Fig. 14~16. Fig. 14 shows the lift distribution for the unswept wing. For the wash-in case ($\theta = 60°$~$75°$), there is large increase in wing loading near a wing tip. For the wash-out

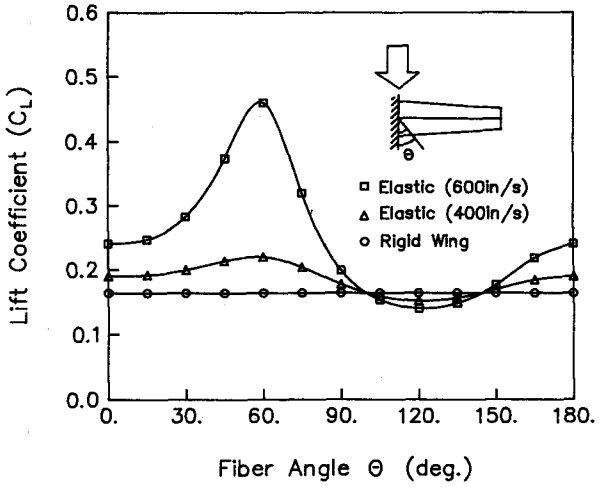

Fig.11 Effect of Fiber Orientation θ upon Lift Coefficient of $[\theta_2/90_2]_S$ Unwept Wing ($\Lambda = 0°$, $\alpha = 2°$)..

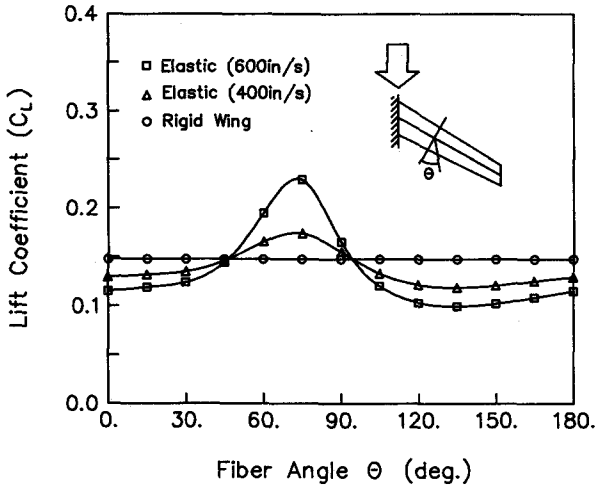

Fig.12 Effect of Fiber Orientation θ upon Lift Coefficient of $[\theta_2/90_2]_S$ Swept Back Wing ($\Lambda = 30°$, $\alpha = 2°$).

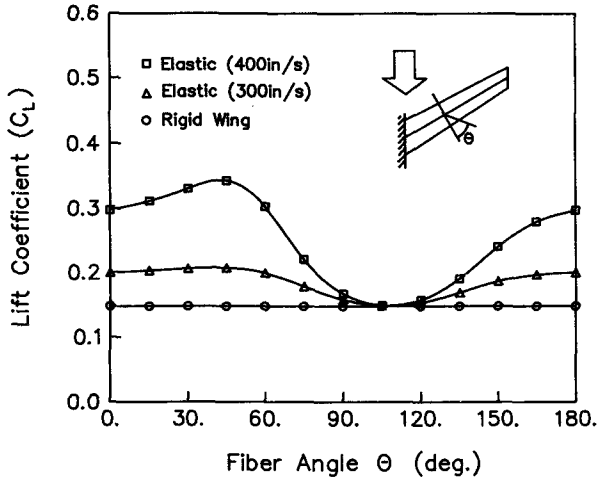

Fig.13 Effect of Fiber Orientation θ upon Lift Coefficient of $[\theta_2/90_2]_S$ Swept Forward Wing ($\Lambda = -30°$, $\alpha = 2°$).

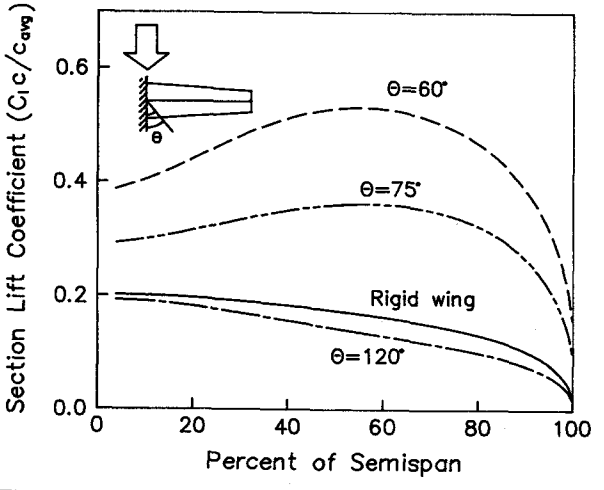

Fig.14 Effect of Fiber Orientation θ upon Spanwise Lift Distribution of $[\theta_2/90_2]_S$ Unwept Wing ($\Lambda = 0°$, U_∞ = 600 in./s, $\alpha = 2°$).

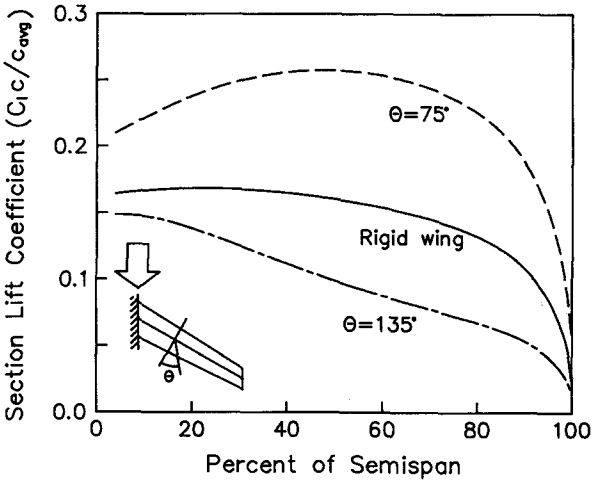

Fig.15 Effect of Fiber Orientation θ upon Spanwise Lift Distribution of $[\theta_2/90_2]_S$ Swept Back Wing ($\Lambda = 30°$, $U_\infty = 600$ in./s, $\alpha = 2°$).

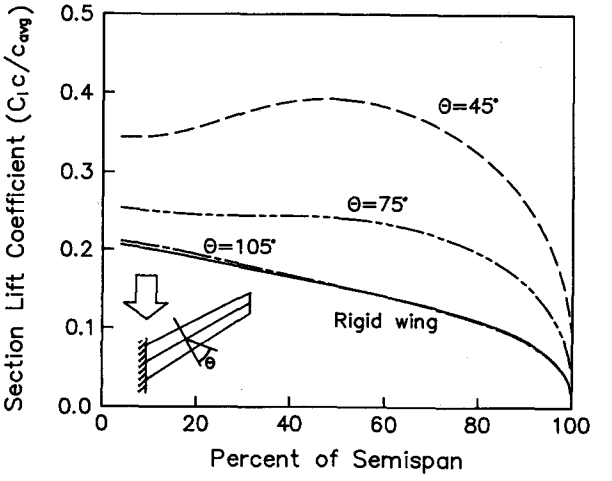

Fig.16 Effect of Fiber Orientation θ upon Spanwise Lift Distribution of $[\theta_2/90_2]_S$ Swept Forward Wing ($\Lambda = -30°$, $U_\infty = 400$ in./s, $\alpha = 2°$).

case ($\theta = 120°$), the overall load decrease is observed. Fig. 15 describes the similar spanwise lift distribution for the 30° swept back wing and Fig. 16 for 30° swept forward wing. It is remarkable that the big change in the spanwise loading mainly occurs in the outer part of the spanwise location.

Concluding Remarks

Three types of composite plate wings (sweep angle 0°,30°, -30°) were analyzed to see the flexibility of composite wings by the finite element method and the vortex lattice method. T300/5208 Gr/Ep composite material of stacking sequence $[\theta_2/90_2]_S$ was used. The effect of fiber orientation, air speed, and sweep angle on the deformation pattern of a wing and aerodynamic load changes were examined. The deformation

patterns are affected by the fiber orientation. For the unswept wing, the typical deformation pattern is wash-in and the wash-out deformation is only observed at θ = 105°~150°. For swept back wing, the typical deformation pattern is wash-out and the wash-in deformation is only observed at θ = 50°~90°. For the swept forward wing, the typical deformation pattern is wash-in and a small wash-out deformation is observed at θ =105°. The optimum wing deformation for all three wings can be obtained at the fiber angle of θ =90°~120°. For the case of the swept forward wing, the wing deformation is very sensitive to velocity changes but the proper selection of composite orientation angle reduces the deformation of the wing noticeably.

References

1. "Static Aeroelasticity in Combat Aircraft," AGARD Rep. 725, Jan. 1986.

2. Weisshaar, T. A., " Divergence of Forward Swept Composite Wings, " *Journal of Aircraft,* Vol. 17, June 1980, pp. 442-448.

3. Bisplinghoff, R. L., Ashley H. and Halfman, R. L., *Aeroelasticity,* Addison-Wesley Pub., Co. 1955.

4. Weisshaar, T. A., " Aeroelastic Tailoring of Forward Swept Composite Wings," *Journal of Aircraft,* Vol. 18, Aug. 1981, pp. 669-676.

5. Hollowell, S. J. and Dugundji, J., "Aeroelastic Flutter and Divergence of Stiffness Coupled, Graphite/Epoxy Cantilevered Plates," *Journal of Aircraft,* Vol. 21, Jan. 1984, pp. 69-76.

6. Lottati, I., " Flutter and Divergence Aeroelastic Characteristics for Composite Forward Swept Cantilevered Wing," *Journal of Aircraft,* Vol. 22, Nov. 1985, pp.1001-1007.

7. Landsberger, B. J., Dugundji, J., " Experimental Aeroelastic Behavior of Unswept and Forward-Swept Cantilever Graphite/Epoxy Wings," *Journal of Aircraft,* Vol. 22, No. 8, Aug. 1985, pp. 679-686.

8. Rowan, J. C., Burns, T. A., " Aeroelastic Loads Predictions Using Finite Element Aerodynamics," *Journal of Aircraft,* Vol. 12, Nov. 1975, pp. 890-898.

9. Sherrer, V. C., Hertz, T. J., Shirk, M.H.," Wind Tunnel Demonstration of Aeroelastic Tailoring Applied to Forward Swept Wings," *Journal of Aircraft,* Vol. 18, Nov. 1981, pp. 976-983.

10. Lin, Kuo-Juin, Lu Pong-Jeu, Tarn, Jiann-Quo, " Flutter Analysis of Composite Plates in Subsonic Flow," *AIAA Journal,* Vol. 27, No. 8, Aug. 1989, pp.1102-1109.

11. Bohlmann, J. D., " Static Aeroelasticity of a Composite Oblique Wing in Transonic Flows," Symposium on Unsteady Transonic Aerodynamics & Aeroelasticity, May 20-22, 1987.

12. Ide, H., Shankar, V. J., "Application of a Fast, Time Accurate Full Potential Scheme to a Statically Flexible Wing in the Transonic Regime," *AIAA Paper* 87-0707, 1987.

13. Tatum, K. E., Giles, G. L., " Integrating Nonlinear Aerodynamic and Structural Analysis for a Complete Fighter Configuration," *Journal of Aircraft,* Vol. 25, No. 12, Dec. 1988, pp. 1150-1156.

14. Bertin, J. J., Smith, M. L., *Aerodynamics for engineers.*, Prentice Hall, Englewood Cliffs, New Jersey, 1979.

15. Harder, R. L., Desmarais, R. N., " Interpolation Using Surface Splines," *Journal of Aircraft,* Vol. 9, No. 2, Feb. 1972, pp. 189-191.

16. Whitney, J.M., *Structural Analysis of Laminated Anisotropic Plates,* Technomic, 1987.

17. Reddy, J. N., *Introduction to Finite Element Method,* McGraw-Hill, 1984.

Appendix

$$K_{ij}^{11} = \int_{\Omega e} \left\{ A_{45}\left(\frac{\partial \psi_j}{\partial y}\frac{\partial \psi_i}{\partial x} + \frac{\partial \psi_j}{\partial x}\frac{\partial \psi_i}{\partial y}\right) + A_{55}\frac{\partial \psi_j}{\partial x}\frac{\partial \psi_i}{\partial x} + A_{44}\frac{\partial \psi_j}{\partial x}\frac{\partial \psi_i}{\partial x} \right\} dxdy$$

$$K_{ij}^{12} = \int_{\Omega e} \left\{ A_{55}\psi_j \frac{\partial \psi_i}{\partial x} + A_{45}\psi_j \frac{\partial \psi_i}{\partial x} \right\} dxdy$$

$$K_{ij}^{13} = \int_{\Omega e} \left\{ A_{45}\psi_j \frac{\partial \psi_i}{\partial x} + A_{44}\psi_j \frac{\partial \psi_i}{\partial x} \right\} dxdy$$

$$K_{ij}^{22} = \int_{\Omega e} \left\{ D_{11}\frac{\partial \psi_j}{\partial x}\frac{\partial \psi_i}{\partial x} + D_{16}\left(\frac{\partial \psi_j}{\partial y}\frac{\partial \psi_i}{\partial x} + \frac{\partial \psi_j}{\partial x}\frac{\partial \psi_i}{\partial y}\right) + D_{66}\frac{\partial \psi_j}{\partial y}\frac{\partial \psi_i}{\partial y} + A_{55}\psi_j\psi_i \right\} dxdy$$

$$K_{ij}^{23} = \int_{\Omega e} \left\{ D_{12}\frac{\partial \psi_j}{\partial y}\frac{\partial \psi_i}{\partial x} + D_{16}\frac{\partial \psi_j}{\partial x}\frac{\partial \psi_i}{\partial x} + D_{26}\frac{\partial \psi_j}{\partial y}\frac{\partial \psi_i}{\partial y} + D_{66}\frac{\partial \psi_j}{\partial x}\frac{\partial \psi_i}{\partial y} + A_{45}\psi_j\psi_i \right\} dxdy$$

$$K_{ij}^{33} = \int_{\Omega e} \left\{ D_{22}\frac{\partial \psi_j}{\partial y}\frac{\partial \psi_i}{\partial y} + D_{26}\left(\frac{\partial \psi_j}{\partial y}\frac{\partial \psi_i}{\partial x} + \frac{\partial \psi_j}{\partial x}\frac{\partial \psi_i}{\partial y}\right) + D_{66}\frac{\partial \psi_j}{\partial x}\frac{\partial \psi_i}{\partial x} + A_{44}\psi_j\psi_i \right\} dxdy$$

$$F_i^1 = \int_{\Omega e} q\psi_i \, dx dy + \int_{\Gamma e} Q_n \psi_i \, ds \,, \quad Q_n = Q_x n_x + Q_y n_y$$

$$F_i^2 = \int_{\Gamma e} M_n \psi_i \, ds \,, \quad M_n = M_x n_x + M_{xy} n_y$$

$$F_i^3 = \int_{\Gamma e} M_{ns} \psi_i \, ds \,, \quad M_{ns} = M_y n_y + M_{xy} n_x$$